Dynamics of a pair of overlapping polar bright solitons in spin-1 Bose-Einstein condensates

Gautam Hegde, Sandra M. Jose, and Rejish Nath
Department of Physics, Indian Institute of Science Education and Research, Dr. Homi Bhabha Road, Pune 411 008, India

(Received 4 May 2022; accepted 28 September 2022; published 11 October 2022)

We analyze the dynamics of both population and spin densities, emerging from the spatial overlap between two distinct polar bright solitons in spin-1 spinor condensates. The dynamics of overlapping solitons in scalar condensates exhibits soliton fusion, atomic switching from one soliton to another, and repulsive dynamics depending on the extent of overlap and the relative phase between the solitons. The scalar case also helps us understand the dynamics of the vector solitons in which the ratio between spin-dependent and spin-independent interaction strengths also plays a vital role. In the absence of spin-changing collisions, we observe Josephson-like oscillations for each spin component leading to the emergence of oscillating domain walls. In the presence of spin-dependent interactions, the overlapping polar solitons may emerge as ferromagnetic solitons or oscillatons or a combination of both. In the end, we discuss the experimental procedure to observe the same dynamics using a rubidium spin-1 Bose-Einstein condensate setup.

DOI: 10.1103/PhysRevA.106.043307

I. INTRODUCTION

Because of spin-dependent interactions, spinor condensates are ideal for exploring coherent spin-mixing dynamics [1–9]. The resulting oscillations in the populations of the Zeeman states can be engineered by varying the initial populations and the relative phases [10]. In a spin-1 condensate, the oscillatory dynamics arises because of the collisional interconversion of two atoms in the $m = 0$ state and one atom each in $m = 1$ and $m = -1$ states. Such a spin-changing process preserves the net magnetization. Further, high controllability over the spin dynamics can be accessed via external magnetic or microwave fields utilizing linear and quadratic Zeeman effects.

Spinor condensates also provide an opportunity to study vector solitons [11–18] in quasi-one-dimensional (Q1D) Bose-Einstein condensates (BECs), including the bright solitons [19–24]. Vector solitons are self-trapped wave packets with multiple components. In spin-1 condensates, the bright solitons are classified into polar and ferromagnetic based on the spin state and the expectation value of the time-reversal operator [24]. Collisional properties of polar-polar, polar-ferromagnetic, and ferromagnetic-ferromagnetic solitons have been studied in the past [20,25] and later led to the discovery of an exotic soliton called the oscillaton [24,26]. Oscillatons are solitons where the total density profile remains stationary while the populations of each m component oscillate in time. It is also possible to observe oscillatory spin dynamics in a special trapped single soliton which is a high-energy eigenstate of the system [27].

In this paper we analyze the dynamics of a pair of overlapping polar bright solitons in spin-1 spinor condensates. Note that the scenario differs from the setups used to study soliton collisions. In the latter case, the solitons are initially placed very far apart and collide against each other with an initial velocity. In our case, the solitons are initially at rest and overlapping. The dynamics of overlapping optical solitons is studied theoretically [28–31] and experimentally [32–35], but a detailed analysis of overlapping matter-wave solitons is lacking. Because of that, we look at the dynamics of overlapping bright solitons in scalar condensates, which helps us understand the unique features emerging from the vectorial nature of the spinor solitons. The dynamics critically depends on the initial phase difference and the extent of overlap between the solitons in the scalar case. The relative phase is expected to play a vital role since it determines the nature of the force between solitons [36–39]. In particular, for a zero phase difference the solitons attract and for a difference of π, they repel. A nonzero phase difference between colliding solitons can dynamically break the symmetry between two solitons [40]. The phase difference also plays a vital role in the stability of colliding three-dimensional solitons [41,42]. For the overlapping scalar matter-wave solitons, we see that, depending on the phase difference, the soliton fusion, atomic flow from one soliton to another, and repulsive dynamics occur. Similar scenarios are found in the dynamics of overlapping optical solitons in different nonlinear media [29,32–34]. In particular, the flow of atoms from one soliton to another mimics the phenomenon of optical switching and we term it atomic switching for the matter-wave solitons.

The vectorial nature of spinor solitons leads to rich dynamics in population and spin densities of spin-1 condensates. Besides the relative phase and the extent of overlap between the solitons, the ratio between the spin-dependent and spin-independent interaction strengths also affects the dynamics significantly. A simplified picture of the dynamics is attained using a rotated frame. In the absence of spin-changing collisions, we observe Josephson-like oscillations in the population dynamics of each spin component. For atoms in each Zeeman state, the Josephson-like oscillations are explained

using an effective potential created by the density of other components. In this case, the population dynamics is independent of the relative phase, but that of the spin-density vector depends on it. The dynamics of the spin-density vector reveals the appearance of oscillating domain walls, depending on the relative phase. When spin-independent and spin-dependent interactions are identical, the collision of a pair of polar solitons results in four ferromagnetic solitons irrespective of the value of the initial relative phase. Among the four ferromagnetic solitons, each pair exhibits dynamics identical to that of scalar solitons that become more apparent in the new rotated frame. When the ratio of spin-dependent and spin-independent interactions is half, we see the formation of a pair of oscillatons. An additional stationary ferromagnetic soliton emerges if the extent of overlap is sufficiently large, depending on the relative phase.

The paper is structured as follows. In Sec. II we discuss the dynamics of overlapping bright solitons in scalar condensates. In Sec. III we discuss the dynamics of overlapping polar solitons in spin-1 condensates. In particular, Sec. III A explains the model of spinor solitons, especially the governing Hamiltonian, the initial state, and time-dependent coupled nonlinear Schrödinger equations in the original and the rotated frame. In Sec. III B we classify the dynamics based on the ratio between the spin-dependent and spin-independent interaction strengths. In particular, the dynamics in the absence of spin-changing collisions is discussed in Sec. III B 1. The dynamics for identical spin-independent and spin-dependent interactions is discussed in Sec. III B 2 and the case when the spin-dependent interaction strength is half of the spin-independent interaction is discussed in Sec. III B 3. Section IV proposes an experimental procedure to observe the dynamics studied in previous sections. We summarize in Sec. V.

II. SCALAR CONDENSATES

In the following, we analyze the dynamics of two identical, overlapping Q1D bright solitons in scalar condensates for different initial relative phases and the extent of overlaps. The analytic form of the initial two-soliton wave function is

$$\psi(z, t=0) = A\left\{\mathrm{sech}\left[k\left(z-\frac{\Delta}{2}\right)\right] + e^{i\phi}\mathrm{sech}\left[k\left(z+\frac{\Delta}{2}\right)\right]\right\}, \quad (1)$$

where ϕ is the relative phase, k is the wave number, Δ is the initial separation between the solitons, which controls the extent of overlap, and the normalization constant is

$$A = \frac{1}{2}\sqrt{\frac{k}{1+k\Delta\cos\phi\,\mathrm{csch}k\Delta}}.$$

For large values of Δ, the solitons do not overlap and remain at rest, maintaining their size and shape over time. Interestingly, a tiny spatial overlap between the solitons can trigger nontrivial dynamics, depending critically on the phase difference. The nature of soliton interactions, whether attractive or repulsive, also depends on their relative phase. The three different relative phases we consider ($\phi = 0,\ \pi/2,$ and $\phi = \pi$ rad) capture the distinct dynamical scenarios of the overlapping

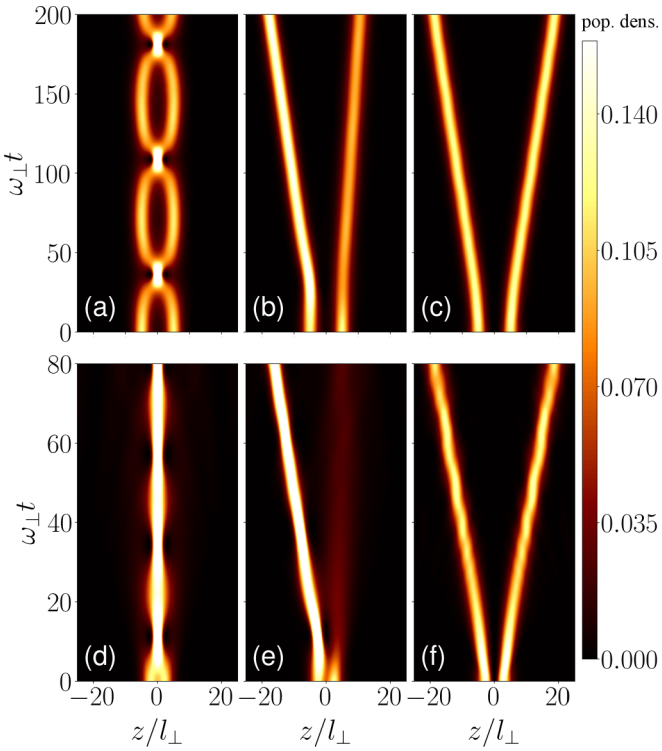

FIG. 1. Population dynamics of two overlapping identical bright solitons in scalar condensates for a different relative phase between them for $g/2\pi\hbar\omega_\perp l_\perp^3 = -2$. The separation is (a)–(c) $\Delta = 10l_\perp$ and (d)–(f) $\Delta = 5l_\perp$ for (a) and (d) $\phi = 0$, where (a) the overlap leads to perpetual oscillating dynamics between the soliton fusion and the initial configuration and (d) the system does not revert completely to the initial configuration; (b) and (e) $\phi = \pi/2$, where an initial atomic flow along the phase gradient leads to asymmetric final solitons; and (c) and (f) $\phi = \pi$, where the solitons repel each other, but are identical in their size and shape.

solitons. For the scalar condensates, the dynamics is governed by the Q1D Gross-Pitaevskii equation (GPE)

$$i\hbar\frac{\partial}{\partial t}\psi(z,t) = \left[-\frac{\hbar^2}{2M}\frac{\partial^2}{\partial z^2} + \frac{g}{2\pi l_\perp^2}|\psi(z,t)|^2\right]\psi(z,t), \quad (2)$$

where $g = 4\pi\hbar^2 a_s N/M$ with the s-wave scattering length $a_s < 0$, N is the total number of particles, and $l_\perp = \sqrt{\hbar/m\omega_\perp}$ is the width of the transverse harmonic confinement of frequency $\omega_\perp$. The wave number k in Eq. (1) depends on the interaction strength via $k = |g|/8\pi\hbar\omega_\perp l_\perp^4$.

When $\phi = 0$, the overlap leads to the attractive interaction between the solitons, making them fuse into a single soliton [43]. Not being in its lowest-energy state, the fused soliton disentangles back into the initial two-soliton configuration if the overlap is sufficiently small [see Fig. 1(a) for $\Delta = 10l_\perp$]. This process repeats periodically in time, leading to the perpetual oscillating dynamics between soliton fusion and the initial configuration as shown in Fig. 1(a). As the initial overlap between the solitons increases (decreasing Δ), the period of oscillation gets shorter [see Fig. 2(a) for the time period T vs Δ]. Strikingly, oscillations in Fig. 1(a) arise in the absence of harmonic confinement, making it in high contrast with those exhibited by trapped solitons [38,42]. Beyond a certain

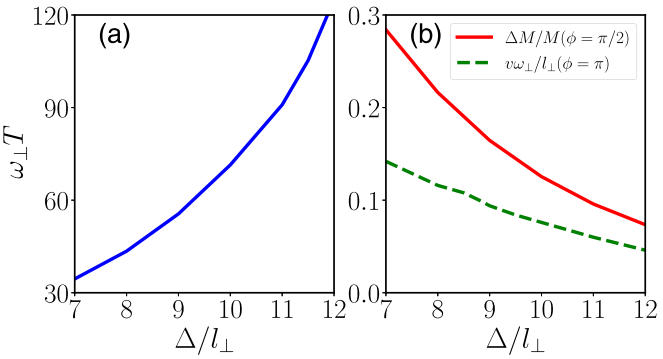

FIG. 2. Soliton properties as a function of Δ for a different initial relative phase for the scalar case and $g/2\pi\hbar\omega_\perp l_\perp^3 = -2$. (a) Time period of oscillations between soliton fusion and the initial configuration for $\phi = 0$. (b) The solid line depicts the mass difference $\Delta M/M$ between the final solitons for $\phi = \pi/2$ rad and the dashed line shows the speed of the final symmetric solitons for $\phi = \pi$ rad.

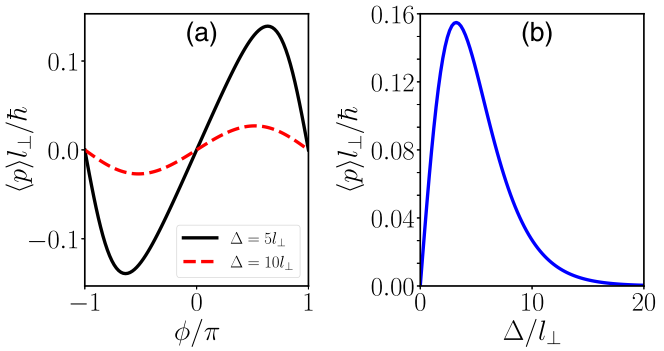

FIG. 3. (a) Average momentum $\langle p\rangle$ as a function of ϕ for $\Delta = 5l_\perp$ (solid line) and $\Delta = 10l_\perp$ (dashed line) and (b) $\langle p\rangle$ vs Δ for $\phi = \pi/2$ rad. In both figures $g/2\pi l_\perp^3\hbar\omega_\perp = -2$.

overlap or smaller Δ, the solitons become nonseparable after the initial fusion as shown in Fig. 1(d) for $\Delta = 5l_\perp$ and the final soliton exhibits breathing dynamics because of the extra energy it carries. These results are found to be similar to that of overlapping optical solitons in plasma [29].

As the initial relative phase between the solitons increases, they repel each other. For instance, when $\phi = \pi/2$ [see Fig. 1(b)], not only do the solitons repel, but also there is a flow of atoms along the direction of the phase gradient, i.e., along $\partial\phi/\partial z$, at the initial stage of the dynamics. This atomic flow is identical to the energy transfer observed among overlapping optical solitons, which leads to the optical switching [32,33]. In a similar spirit, the atom transfer from one soliton to another can serve as a control knob to direct the motion of matter waves. Hence we call it atomic switching. In Fig. 1(b) the atomic flow occurs from the positive z direction to the negative one. Such a transient atomic current makes the final solitons asymmetric in density, size, and speed. The denser soliton moves faster. The momentum of the lighter soliton arises from the recoil of the atoms flown out from the original soliton. To quantify the mass asymmetry of the final solitons, we introduce the mass difference between the left and right solitons, i.e., $\Delta M = M_l - M_r$, where $M_l = M\int_{-\infty}^{0}|\psi(z,t)|^2dz$ and $M_r = M\int_0^{\infty}|\psi(z,t)|^2dz$. In Fig. 2(b) the solid line shows ΔM obtained when the solitons are well separated after a sufficiently long time. As can be seen, ΔM increases with decreasing Δ because the larger the initial overlap the more significant the exchange of atoms. The atomic switching is evident in Figs. 1(b) and 1(e) for $\Delta = 10l_\perp$ and $5l_\perp$, respectively.

The asymmetry of final solitons implies that there is a net momentum in the system for $\phi = \pi/2$. To quantify that, we calculate the average momentum of the initial wave function in Eq. (1),

$$\langle p\rangle = 4A^2(1 - k\Delta\coth k\Delta)\mathrm{csch}k\Delta\sin\phi. \tag{3}$$

In Fig. 3(a) we show $\langle p\rangle$ as a function of ϕ for $\Delta = 10l_\perp$ and $5l_\perp$, which oscillates between positive and negative values as a function of ϕ. Thus, by tuning the relative phase, we can control the direction of the transient atomic current or, equivalently, the direction of the atomic switching. For $\phi = 0$, $\langle p\rangle = 0$ as expected. For $\phi = \pi/2$ rad, $\langle p\rangle$ exhibits a nonmonotonic behavior as a function of Δ, exhibiting a local maximum, as shown in Fig. 3(b). At $\Delta = 0$, the solitons completely overlap and remain at rest; thus $\langle p\rangle = 0$. Also, as $\Delta \to \infty$, $\langle p\rangle$ approaches zero as both solitons become completely independent.

The solitons also repel each other for $\phi = \pi$ [see Figs. 1(c) and 1(f)], but there is no transient atomic current due to the nodal point at $z = 0$. Hence, the final solitons are identical and $\Delta M = 0$. The final solitons propagate with equal and opposite velocity. The final speed v of the soliton vs Δ for $\phi = \pi$ rad is shown as a dashed line in Fig. 2(b). The more initial overlap the solitons have, the faster they move away from each other. Summarizing this section, we see that the initial phase difference and the extent of overlap critically affect the dynamics of overlapping bright solitons in scalar condensates. The most interesting feature is the local and transient atomic current due to an effective repulsion arising from the phase difference between the solitons. This scenario is identical to optical switching, offering the possibility of engineering matter-wave transport via controlling the relative phase.

III. SPIN-1 SPINOR CONDENSATES

A. Setup, model, initial state, and rotated frame

The systems we consider are overlapping spin-1 condensates, described by the Hamiltonian

$$\hat{H} = \int dz\left[-\frac{\hbar^2}{2M}\sum_m \hat{\psi}_m^\dagger\frac{d^2}{dz^2}\hat{\psi}_m + \frac{1}{2}\bar{c}_0 : \hat{n}^2 : + \frac{1}{2}\bar{c}_1 : \hat{\boldsymbol{F}}^2 :\right], \tag{4}$$

where M is the mass of a boson, $\bar{c}_{0,1} = c_{0,1}/2\pi l_\perp^2$ are the interaction parameters, $\hat{\psi}_m$ is the field operator which annihilates a boson of the mth Zeeman state, and $\hat{n}(z) = \sum_{m=-f}^{f}\hat{\psi}_m^\dagger(z)\hat{\psi}_m(z)$ is the total density operator. The components of the spin-density operator are

$$\hat{F}_{v\in x,y,z}(z) = \sum_{m,m'}(f_v)_{mm'}\hat{\psi}_m^\dagger(z)\hat{\psi}_{m'}(z), \tag{5}$$

with f_v the vth component of the spin-1 matrices. The symbol : : denotes the normal ordering that places annihilation

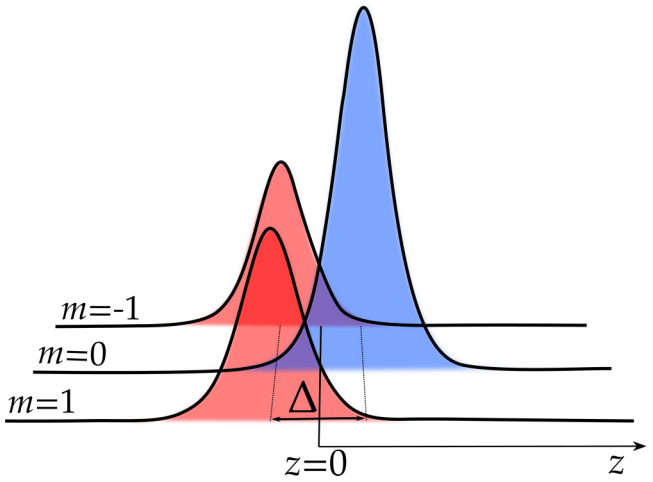

FIG. 4. Schematic setup of overlapping bright polar solitons in Q1D spin-1 condensates, along the z axis. A polar soliton with population shared among $m = \pm 1$ states is shown on the left (red-shaded area) and a polar soliton with population solely at $m = 0$ is on the right side (blue-shaded area). The separation Δ determines the extent of overlap between the two solitons.

operators to the right of the creation operators. The spin-independent and spin-dependent interaction parameters are $c_0 = (g_0 + 2g_2)/3$ and $c_1 = (g_2 - g_0)/3$, respectively, with $g_{\mathcal{F}} = 4\pi\hbar^2 a_{\mathcal{F}} N/m$ related to the scattering length $a_{\mathcal{F}=0,\,2}$ of the total spin-$\mathcal{F}$ channel. Here N is the total number of atoms. To have bright solitons, we keep $c_0 < 0$.

Within the mean-field theory, the dynamics of the system is described by the Q1D GPEs [19,20,26]

$$i\hbar\frac{\partial\psi_1}{\partial t} = \left[-\frac{\hbar^2}{2M}\frac{\partial^2}{\partial z^2} + \bar{c}_0 n + \bar{c}_1 F_z\right]\psi_1 + \frac{\bar{c}_1}{\sqrt{2}}F_-\psi_0, \quad (6)$$

$$i\hbar\frac{\partial\psi_0}{\partial t} = \left[-\frac{\hbar^2}{2M}\frac{\partial^2}{\partial z^2} + \bar{c}_0 n\right]\psi_0 + \frac{\bar{c}_1}{\sqrt{2}}F_+\psi_1 + \frac{\bar{c}_1}{\sqrt{2}}F_-\psi_{-1}, \quad (7)$$

$$i\hbar\frac{\partial\psi_{-1}}{\partial t} = \left[-\frac{\hbar^2}{2M}\frac{\partial^2}{\partial z^2} + \bar{c}_0 n - \bar{c}_1 F_z\right]\psi_{-1} + \frac{\bar{c}_1}{\sqrt{2}}F_+\psi_0, \quad (8)$$

where $n(z,t) = \sum_m |\psi_m(z,t)|^2$ is the total density, $F_\nu(z,t) = \sum_{m,m'} \psi_m^*(\mathrm{f}_\nu)_{\mathrm{mm'}}\psi_{\mathrm{m'}}$, and $F_\pm = F_x \pm iF_y$. We introduce $\gamma = -c_1/|c_0|$ as the ratio of spin-dependent and spin-independent interactions. A positive (negative) γ implies a negative (positive) c_1. Here we take $c_1 \leqslant 0$ (ferromagnetic interactions) and study the dynamics. The validity of Eqs. (6)–(8) requires that $\mu_{1\mathrm{D}} \ll \hbar\omega_\perp$, where $\omega_\perp$ is the transverse confinement frequency and $\mu_{1\mathrm{D}}$ is the chemical potential of the Q1D condensates. We solve Eqs. (6)–(8) numerically to analyze the dynamics [44]. At $\gamma = 1$, Eqs. (6)–(8) represent a completely integrable system and support N-soliton solutions including two-soliton ones [19].

Initial state. The schematic diagram of the initial state is shown in Fig. 4, in which two distinct polar solitons overlap around $z = 0$. The general solution of a static polar soliton is

$$\psi(z) = \sqrt{\frac{k}{2}}\chi\,\mathrm{sech}\,kz, \quad (9)$$

where $k = |\bar{c}_0|/4l_\perp$ is the inverse width or the wave number of the soliton wave packet and χ is the spin state, which takes the general form [24,26]

$$\chi = e^{i\tau}\begin{pmatrix} -\frac{1}{\sqrt{2}}\sin\theta \\ \cos\theta \\ \frac{1}{\sqrt{2}}e^{i\phi}\sin\theta \end{pmatrix}, \quad (10)$$

where τ is a global phase. Equation (9) is a stationary solution of the Q1D GPEs (6)–(8). The initial state of our studies is a pair of overlapping polar solitons

$$\psi_{\mathrm{in}}(z) = A\left\{\mathrm{sech}\left[k\left(z + \frac{\Delta}{2}\right)\right]\chi_l + \mathrm{sech}\left[k\left(z - \frac{\Delta}{2}\right)\right]\chi_r\right\}, \quad (11)$$

where $A = \sqrt{k}/2$ is the normalization constant and $\chi_r = (0, e^{i\phi_1}, 0)^T$ and $\chi_l = (1, 0, e^{i\phi_2})^T/\sqrt{2}$ are the spin states of the solitons to the right and left of $z = 0$, respectively. Comparing to Eq. (10), $\theta = \pi/2$ for the left soliton and $\theta = 0$ for the right. The angle ϕ_1 is the initial phase of the right soliton and ϕ_2 is the relative phase between the $m = 1$ and $m = -1$ components of the left soliton. The extent of the overlap between the solitons is again controlled by Δ. Note that, for Eq. (11), $\langle p\rangle = 0$ irrespective of Δ and ϕ_1. The experimental procedure to prepare the initial state in Eq. (11) is discussed in Sec. IV.

The spin-density vector is a null vector for each of the polar solitons in Eq. (11) [19,20,24]. When two distinct polar solitons overlap, the spin density may become nonzero in the overlapping region. For the initial state in Eq. (11), the local spin-density vector is

$$\mathbf{F}(z, t = 0) = \frac{4A^2\cos\left(\phi_1 - \frac{\phi_2}{2}\right)}{\cosh 2kz + \cosh k\Delta}\left(\hat{x}\cos\frac{\phi_2}{2} + \hat{y}\sin\frac{\phi_2}{2}\right). \quad (12)$$

The vector $\mathbf{F}(z, t = 0)$ lies in the xy plane and forms an angle ϕ_2 with the x axis. The orientation of $\mathbf{F}(z, t = 0)$ is the same at every point along the z axis and depends only on ϕ_2. The relative angle $\phi_1 - \frac{\phi_2}{2}$ determines the magnitude of $\mathbf{F}(z, t = 0)$ and the net magnetization. Integrating over z, we obtain the net spin-density vector

$$\mathbf{F}_T = 4A^2\Delta\cos\left(\phi_1 - \frac{\phi_2}{2}\right)\mathrm{csch}k\Delta\left(\hat{x}\cos\frac{\phi_2}{2} + \hat{y}\sin\frac{\phi_2}{2}\right), \quad (13)$$

which is a conserved quantity. Without loss of generality, we set $\phi_2 = 0$, which fixes the direction of $\mathbf{F}_T$ along the x axis. We analyze the dynamics for $\phi_1 = 0$, $\pi/2$, and π rad. For $\phi_1 = 0$ and π rad, the initial spin-density vector is along the positive and negative x axes, respectively, whereas for $\phi_1 = \pi/2$ rad, $\mathbf{F}(z, t = 0)$ vanishes. The spin mixing takes place in the overlapping region and leads to interesting dynamical scenarios, which we classify based on the values of γ and ϕ_1.

Rotated frame. Since $\mathbf{F}_T$ is a conserved quantity, it is more favorable to work using a frame in which the quantization axis is parallel to $\mathbf{F}_T$ [27], which may provide a simplified picture

for the dynamics. A similar rotated frame is used in [24,26] to describe oscillatons formed by the collision between a ferromagnetic and a polar soliton. In our case, the new frame is obtained by a rotation of $\pi/2$ about the y axis ($\chi' = e^{i\pi f_y/2}\chi$). The relations between the new and old spinor components are

$$\psi_1'(z) = \frac{1}{2}\psi_1(z) + \frac{1}{\sqrt{2}}\psi_0(z) + \frac{1}{2}\psi_{-1}(z), \tag{14}$$

$$\psi_0'(z) = -\frac{1}{\sqrt{2}}\psi_1(z) + \frac{1}{\sqrt{2}}\psi_{-1}(z), \tag{15}$$

$$\psi_{-1}'(z) = \left(\frac{1}{2}\psi_1(z) - \frac{1}{\sqrt{2}}\psi_0(z) + \frac{1}{2}\psi_{-1}(z)\right). \tag{16}$$

In our case, at any instant, ψ_1 and ψ_{-1} are identical, making $\psi_0'(z)$ vanish completely. The system effectively reduces to a two-component condensate in the new frame [45]. The corresponding GPEs are

$$i\hbar\frac{\partial\psi_{\pm1}'}{\partial t} = \left[-\frac{\hbar^2}{2M}\frac{\partial^2}{\partial z^2} + \bar{c}_+|\psi_{\pm1}'|^2 + \bar{c}_-|\psi_{\mp1}'|^2\right]\psi_{\pm1}', \tag{17}$$

where $\bar{c}_\pm = \bar{c}_0 \pm \bar{c}_1$. The exchange coupling between ψ_1' and ψ_{-1}' is provided by $\bar{c}_0 - \bar{c}_1$. When $\gamma = 1$, $\bar{c}_0 - \bar{c}_1$ vanishes, indicating that the system effectively reduces to two independent scalar condensates in the rotated frame.

B. Dynamics

A comprehensive study of the dynamics of overlapping polar solitons as a function of Δ, γ, and ϕ_1 is a tedious task. We restrict the analysis to $\phi_1 \in \{0, \pi/2, \pi\}$ rad, $\Delta \in \{5l_\perp, 10l_\perp\}$, and $0 \leqslant \gamma \leqslant 1$, in particular, (i) $\gamma = 0$, (ii) $\gamma = 1$, and (iii) $\gamma = 0.5$, which capture the most exciting scenarios. Since $\gamma \geqslant 0$, we have $c_1 \leqslant 0$.

1. Case $\gamma = 0$

First, we discuss the case for which there are no spin-changing collisions, i.e., $\gamma = 0$. In this case, the total population in each Zeeman component remains constant and the population dynamics is independent of ϕ_1. We also find that changing Δ does not affect the dynamics qualitatively. The dynamics for $\gamma = 0$ and $\Delta = 10l_\perp$ is shown in Fig. 5. In particular, Figs. 5(a)–5(c) show the dynamics of $|\psi_1|^2 + |\psi_{-1}|^2$, $|\psi_0|^2$, and the total density $n(z,t)$, respectively. Effectively, we observe Josephson-like oscillations of populations in each component [see Figs. 5(a) and 5(b)] between the two regions (to the left and right of $z = 0$) where the solitons are initially placed. The oscillations are nonsinusoidal. The density oscillations may give a false impression that spin-changing collisions are taking place. To demonstrate the Josephson-like oscillations, for each Zeeman state, we introduce the population imbalance between the left and right sides of $z = 0$, i.e.,

$$Z_m(t) = \frac{1}{N_m}\left(\int_{-\infty}^{0} dz|\psi_m|^2 - \int_{0}^{\infty} dz|\psi_m|^2\right), \tag{18}$$

where N_m is the total number of atoms in the mth state, which is a constant.

The density oscillations of each component can be intuitively understood via an effective potential created by other components. First consider the population dynamics of the

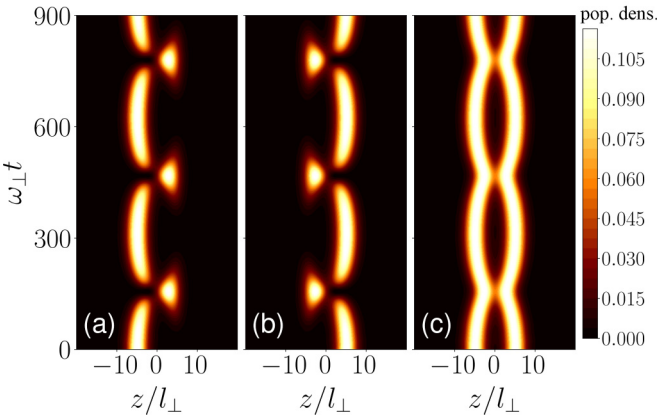

FIG. 5. Population dynamics of two overlapping polar bright solitons for $\gamma = 0$, $\Delta = 10l_\perp$, and $\bar{c}_0/\hbar\omega_\perp l_\perp = -2$: (a) $|\psi_1|^2 + |\psi_{-1}|^2$, (b) $|\psi_0|^2$, and (c) total density $n(z,t)$. The results are independent of the value of ϕ_1.

$m = 1$ state, which is shown in Fig. 5(a) (identical for the $m = -1$ state). Since most of the population in $m = 1$ is initially to the left of $z = 0$, we have $Z_1(t = 0) \sim 1$. For $\bar{c}_0 < 0$, the terms $\bar{c}_0|\psi_{-1}|^2$ and $\bar{c}_0|\psi_0|^2$ in Eq. (6) form a double-well potential for atoms occupying the $m = 1$ state [see Fig. 6(a) for $V_{\rm eff}^{m=1}(z,t) = \bar{c}_0(|\psi_0|^2 + |\psi_{-1}|^2)$ at different times]. A nonzero fraction of $m = 1$ atoms in the right region triggers the tunneling from left to right, leading eventually to oscillatory dynamics shown in Fig. 5(a). At $t = 0$, $V_{\rm eff}^{m=1}$ is asymmetric in z since the $m = 0$ population on the right side is twice that of the $m = -1$ state on the left. As time evolves, $V_{\rm eff}^{m=1}$ gets modified and the two minima get closer to each

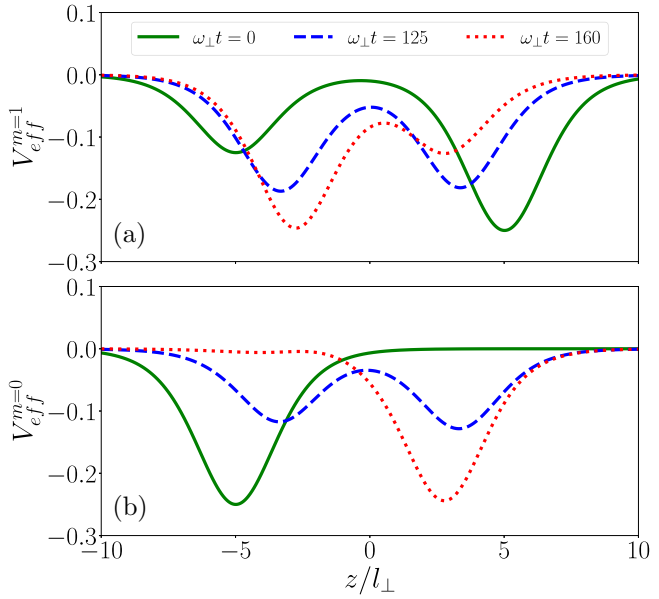

FIG. 6. Effective potential $V_{\rm eff}^m$ generated for the mth component by other components for $\gamma = 0$, $\Delta = 10l_\perp$, and $\bar{c}_0/\hbar\omega_\perp l_\perp = -2$. (a) Here $V_{\rm eff}^{m=1}$ exhibits a double-well potential with its local minima and separation between them varying in time. (b) Here $V_{\rm eff}^{m=0}$ oscillates in time between a single minimum and double minima. The results are independent of the value of ϕ_1.

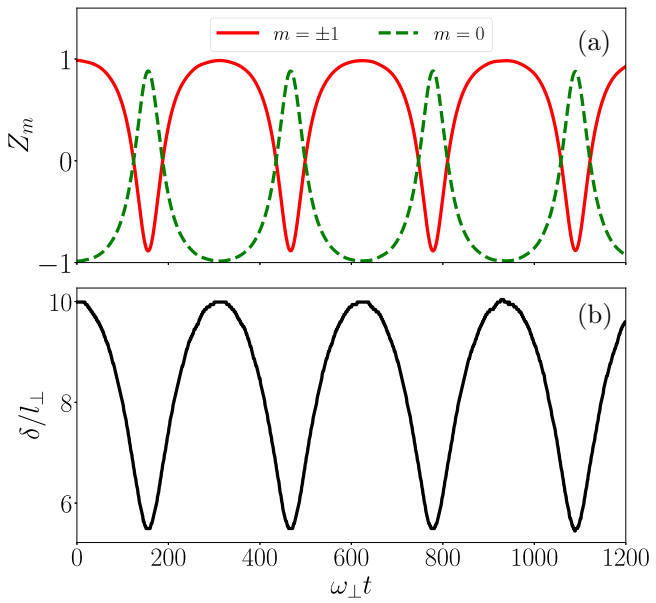

FIG. 7. Dynamics of (a) the population imbalance Z_m and (b) the separation $\delta(t)$ between the two peaks in the total density $\gamma = 0$, $\Delta = 10l_\perp$, and $\bar{c}_0/\hbar\omega_\perp l_\perp = -2$. The results are independent of the value of ϕ_1.

other [see the dashed line in Fig. 6(a)], which amplifies the tunneling rate. Eventually, the potential gets inverted, with a shorter separation between the minima, as shown by the dotted line in Fig. 6(a). The potential gets inverted because of the swapping of population in $m = 0$ ($m = -1$) from left (right) to right (left). By this time, most of the population in the $m = 1$ state has already tunneled to the right. Then the reverse dynamics happens and the system recovers to the initial configuration. The whole process repeats periodically in time.

The population in $m = 0$, initially placed on the right side, experiences a different dynamical potential $[V_{\rm eff}^{m=0}(z,t) = \bar{c}_0(|\psi_1|^2 + |\psi_{-1}|^2)]$ because of the $m = \pm 1$ densities, as shown in Fig. 6(b). As time evolves, the potential minimum, initially on the left (solid line), moves to the right via a transient double-well potential and then reverts. The $m = 0$ atoms always move towards the potential minimum in the opposite region, leading to the oscillatory dynamics shown in Fig. 5(b). Also, note that the $m = \pm 1$ populations remain immiscible with the $m = 0$ component for the entire time, except in the overlapping region. The total density is characterized by the out-of-phase oscillatory dynamics of the two peaks [see Fig. 5(c)].

The Josephson-like dynamics is more apparent in the population imbalance Z_m shown in Fig. 7(a), which exhibits an oscillatory behavior for each component. Figure 7(b) shows the separation δ between the two peaks in the total density or equivalently the distance between the two minima in the effective potential $V_{\rm eff}^{m=1}(z,t)$ [see Fig. 5(c)]. At $t = 0$, $\delta = \Delta$ and over time it varies periodically. The population dynamics becomes faster as δ gets smaller and vice versa. It can be seen in Fig. 7(a) that the population of each component in the initial region never vanishes. Therefore, some atoms are always in the $m = \pm 1$ states in the left region and $m = 0$ in the right region, which helps the system periodically recover to the initial density configurations.

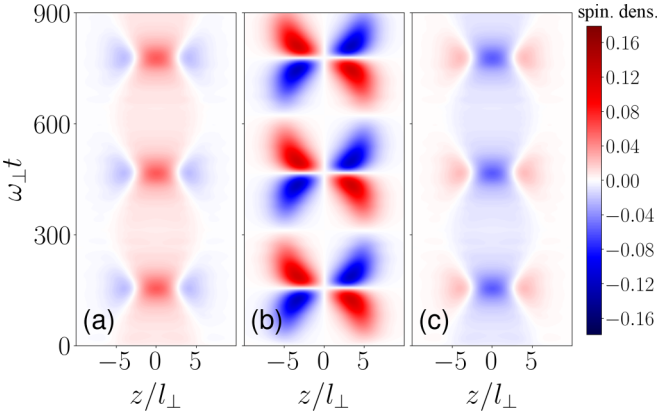

FIG. 8. Dynamics of spin density $F_x(z,t)$ for (a) $\phi_1 = 0$, (b) $\phi_1 = \pi/2$ rad, and (c) $\phi_1 = \pi$ rad. The other parameters are $\gamma = 0$, $\Delta = 10l_\perp$, and $\bar{c}_0/\hbar\omega_\perp l_\perp = -2$.

Even though the population dynamics shown in Fig. 5 is independent of ϕ_1, it affects the spin-density vector $\mathbf{F}(z, t = 0) = F_x(z,t)\hat{x}$ via Eq. (12) and hence its dynamics. In Figs. 8(a)–8(c) we show the dynamics of $F_x(z,t)$ for $\phi_1 = 0$, $\pi/2$, and π rad, respectively. Having $F_x(z,t) \propto (\psi_1 + \psi_{-1})\psi_0^* + (\psi_1^* + \psi_{-1}^*)\psi_0$, the spin-density vector is significant only in the overlapping regions. For $\phi_1 = 0$, $F_T = \int_{-\infty}^{\infty} F_x(z,t)dz$ is positive, i.e., the effective spin is pointing in the positive x direction. At $t = 0$, the spin-density vector is along the x axis at every point in the overlapping region. As time progresses, we observe the formation of domains with positive and negative F_x. In particular, regions of negative values of F_x emerge from the edges of the overlapping region, separated by a region of positive F_x [see Fig. 8(a)]. The domain walls, which separate the positive and negative F_x regions, move towards the center, squeezing the region of positive F_x in the middle. The latter results in an increase in spin density at the center. Because of the conservation of $\mathbf{F}_T$ and energy, they cannot reach beyond a separation. Eventually, the domain walls move back to the edges,and their position oscillates in time. For $\phi_1 = \pi$ rad, the dynamics of $F_x(z,t)$ is identical to that of $\phi_1 = 0$ except that positive and negative regions are swapped [see Fig. 8(c)].

The dynamics of $F_x(z,t)$ for $\phi_1 = \pi/2$ rad is drastically different from that of $\phi_1 = 0$ and π rad [see Fig. 8(b)]. For $\phi_1 = \pi/2$ rad, $F_x(z,0)$ vanishes and hence F_T vanished too. As time progresses, we see simultaneous growth of equal regions of positive and negative F_x. The growth happens from the edges of the overlapping region, separated by a region with $F_x = 0$. As time progresses, the size of the $F_x = 0$ region shrinks and that of $F_x \neq 0$ grows. After some time, surprisingly, $F_x(z,t)$ vanishes quite rapidly at all z and reemerges with opposite polarity. Then the central region with $F_x = 0$ grows until the regions of $F_x \neq 0$ on either side diminish. The whole process repeats periodically in time, leading to the butterfly pattern in space-time shown in Fig. 8(b). The above results indicate that, in the absence of spin-independent interactions, we can engineer the spin dynamics in spinor condensates, while the population dynamics remains unaffected by varying the relative phase ϕ_1.

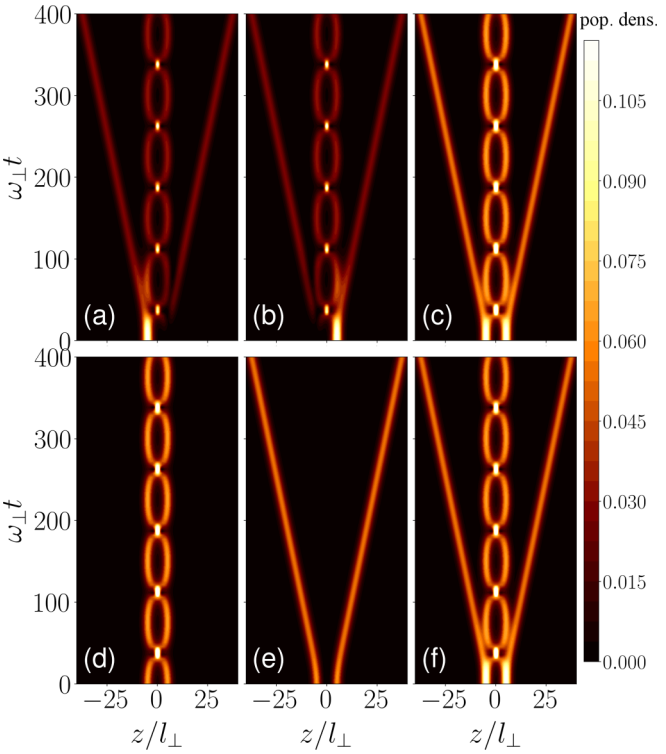

FIG. 9. Population dynamics of two overlapping polar bright solitons for $\gamma = 1$, $\Delta = 10l_\perp$, $\bar{c}_0/\hbar\omega_\perp l_\perp = -2$, and $\phi_1 = 0$: (a) $|\psi_1|^2 + |\psi_{-1}|^2$, (b) $|\psi_0|^2$, (c) total density $n(z,t)$, (d) $|\psi_1'|^2$, (e) $|\psi_{-1}'|^2$, and (f) total density $n'(z,t) = |\psi_1'|^2 + |\psi_{-1}'|^2$. Note that $n(z,t) = n'(z,t)$.

2. *Case* $\gamma = 1$

The presence of spin-changing collisions affects the dynamics drastically. For $\gamma = 1$, spin-dependent and spin-independent interactions are of equal strength and the system is integrable [19]. In Figs. 9(a)–9(c) we show the dynamics of $|\psi_1|^2 + |\psi_{-1}|^2$, $|\psi_0|^2$, and the total density $n(z,t)$, respectively, for $\gamma = 1$, $\Delta = 10l_\perp$, and $\phi_1 = 0$. The first visible effect of the spin-changing collision is that all Zeeman components become spatially miscible, leading to identical density patterns for all Zeeman components at longer times. After a sufficiently long time, the initial overlapping polar solitons convert into four solitons via spin-changing collisions, two each on either side of $z = 0$. Each soliton is characterized by a population ratio of 1:2:1 among the Zeeman states ($m = -1$, 0, and 1) with a spin state $\chi = (1, \pm\sqrt{2}, 1)^T/2$. The latter is a ferromagnetic soliton [24,26]. The spin-density vector shown in Fig. 10(a) confirms that the final solitons are ferromagnetic and have opposite polarity for the inner and outer solitons. The inner solitons have $F_x(z,t) > 0$, i.e., the polarization axis is along the positive x axis, whereas that of outer solitons is along the negative x axis. Thus, we have a scenario where two overlapping polar solitons dynamically convert into four ferromagnetic solitons.

In the rotated frame [Eqs. (14)–(16)], the dynamics looks relatively simple and also provides more insights. Recall that for $\gamma = 1$, the wave functions $\psi_1'(z)$ and $\psi_{-1}'(z)$ are decoupled and effectively we have two independent scalar condensates.

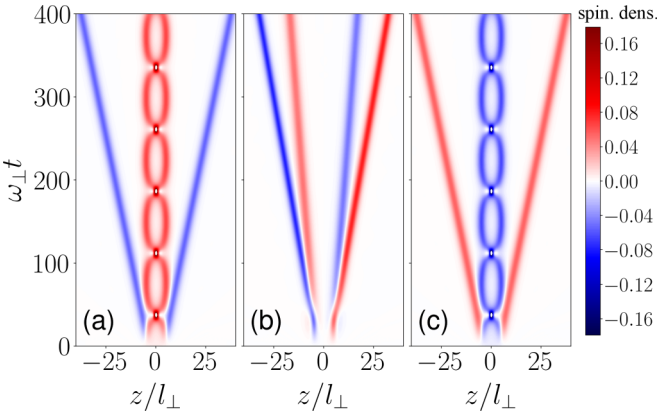

FIG. 10. Dynamics of spin density $F_x(z,t)$ for (a) $\phi_1 = 0$, (b) $\phi_1 = \pi/2$ rad, and (c) $\phi_1 = \pi$ rad. The other parameters are $\gamma = 1$, $\Delta = 10l_\perp$, and $\bar{c}_0/\hbar\omega_\perp l_\perp = -2$.

At $t = 0$, the initial states in the rotated frame with $\phi_1 = 0$ are

$$\psi_{\pm1}'(z) = \frac{\sqrt{k}}{2}\left[\frac{\text{sech}\,[k(z-\Delta/2)]}{\sqrt{2}} \pm \frac{\text{sech}\,[k(z+\Delta/2)]}{\sqrt{2}}\right]. \tag{19}$$

Equation (19) represents scalar two-soliton states, identical to Eq. (1), with relative phases $\phi = 0$ and π rad between the solitons. Comparing the results of the original and the rotated frames in Fig. 9, we see that $|\psi_1'(z,t)|^2$ provides the dynamics of the two inner solitons [see Fig. 9(d)] and $|\psi_{-1}'(z,t)|^2$ gives that of the two outer solitons [see Fig. 9(e)]. They both match with the dynamics of scalar solitons shown in Figs. 1(a) and 1(c), respectively, for the inner and outer solitons. Depending on the extent of the initial overlap, the inner and outer solitons have different masses. The ratio of masses between the inner and outer solitons can be easily obtained via the wave functions in the rotated frame as

$$\frac{\int_{-\infty}^{\infty}|\psi_1'|^2dz}{\int_{-\infty}^{\infty}|\psi_{-1}'|^2dz} = \frac{1 + k\Delta\,\text{csch}k\Delta}{1 - k\Delta\,\text{csch}k\Delta}.$$

Thus, the extent of overlap provides a knob to control the size of the inner and outer ferromagnetic solitons.

The population dynamics for $\phi_1 = \pi$ rad is identical to that of $\phi_1 = 0$ as discussed above, but the spin densities of inner and outer solitons are now flipped [compare Figs. 10(a) and 10(c)]. For $\phi_1 = \pi/2$ rad, the population and spin-density dynamics are qualitatively different from the $\phi_1 = 0$ case. The population dynamics for $\phi_1 = \pi/2$ rad is shown in Fig. 11 and the corresponding spin-density dynamics is shown in Fig. 10(b). After the initial spin-mixing dynamics, again we have four ferromagnetic solitons. Unlike the $\phi_1 = 0$ case, all of them move away from the center. Due to the initial phase difference of $\pi/2$, it takes more time to reach a miscible state, as seen in Figs. 11(a)–11(c), via transient oscillatory dynamics. The initial states in the rotated frame for $\phi_1 = \pi/2$ rad are

$$\psi_{\pm1}'(z) = \frac{\sqrt{k}}{2}\left[\frac{\text{sech}\,[k(z+\Delta/2)]}{\sqrt{2}} \pm \frac{i\text{sech}\,[k(z-\Delta/2)]}{\sqrt{2}}\right], \tag{20}$$

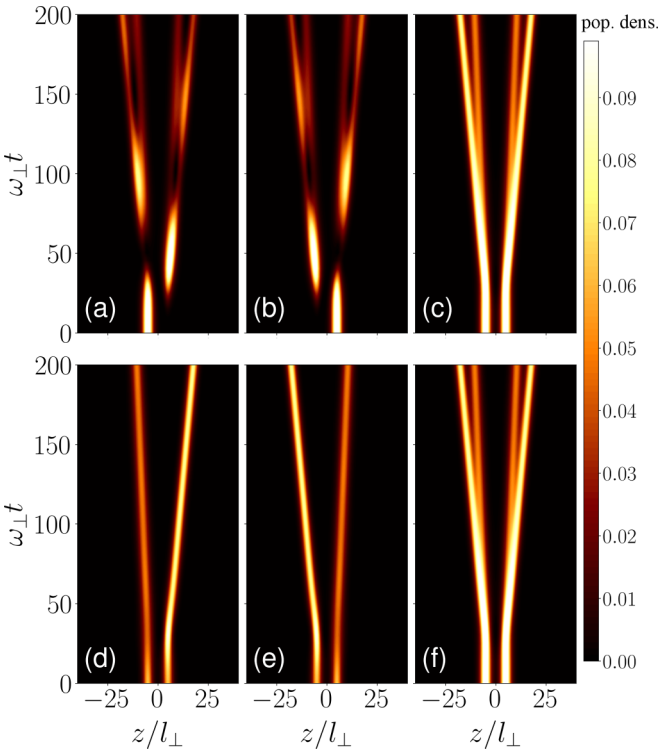

FIG. 11. Population dynamics of two overlapping polar bright solitons for $\gamma = 1$, $\Delta = 10l_\perp$, $\bar{c}_0/\hbar\omega_\perp l_\perp = -2$, and $\phi_1 = \pi/2$ rad: (a) $|\psi_1|^2 + |\psi_{-1}|^2$, (b) $|\psi_0|^2$, (c) total density $n(z,t)$, (d) $|\psi_1'|^2$, (e) $|\psi_{-1}'|^2$, and (f) total density $n'(z,t) = |\psi_1'|^2 + |\psi_{-1}'|^2$. Note that $n(z,t) = n'(z,t)$.

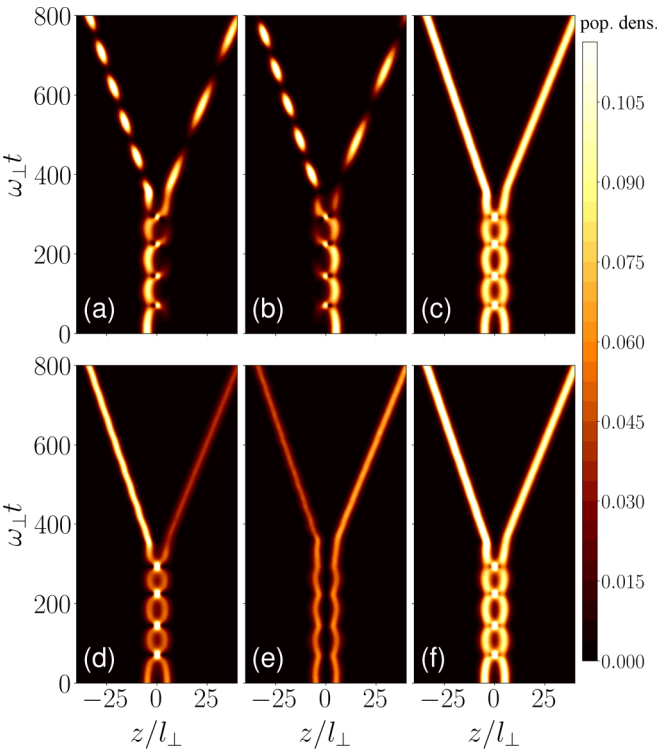

FIG. 12. Population dynamics of two overlapping polar bright solitons for $\gamma = 0.5$, $\Delta = 10l_\perp$, $\bar{c}_0/\hbar\omega_\perp l_\perp = -2$, and $\phi_1 = 0$: (a) $|\psi_1|^2 + |\psi_{-1}|^2$, (b) $|\psi_0|^2$, (c) total density $n(z,t)$, (d) $|\psi_1'|^2$, (e) $|\psi_{-1}'|^2$, and (f) total density $n'(z,t) = |\psi_1'|^2 + |\psi_{-1}'|^2$. Note that $n(z,t) = n'(z,t)$.

representing two independent two-soliton solutions but with opposite phase gradients. As we know from the scalar case for $\phi = \pi/2$ rad [see Figs. 1(b) and 1(e)], there is a transient atomic current along the direction of the phase gradient. Therefore, in $\psi_1'(z)$, the current is from left to right and in $\psi_{-1}'(z)$ it is from right to left. That results in a pair of asymmetric solitons in both $\psi_1'(z)$ and $\psi_{-1}'(z)$. Since the denser solitons move faster, the inner solitons are lighter, in contrast to the $\phi_1 = 0$ case where all solitons are identical. As seen in Fig. 10(b), the spin vectors point in opposite directions among the inner and the outer solitons. Again, by tuning Δ, we can control the mass ratio between the inner and outer solitons and also the frequency of transient oscillation seen in the initial stage of the dynamics in Figs. 11(a) and 11(b).

3. *Case* $\gamma = 0.5$

In the following, we analyze the dynamics for $\gamma = 0.5$ and observe the emergence of a pair of nonidentical oscillatons propagating in opposite directions. Oscillatons are solitons in which the total density profile remains stationary while the populations of different spin components oscillate with a constant frequency [24,26]. In Figs. 12(a)–12(c) we show the dynamics of $|\psi_1|^2 + |\psi_{-1}|^2$, $|\psi_0|^2$, and the total density $n(z,t)$, respectively, for $\gamma = 0.5$, $\Delta = 10l_\perp$, and $\phi_1 = 0$. In the initial stage, spin mixing leads to oscillatory dynamics. Later, the condensates transform into a pair of nonidentical oscillatons moving in opposite directions. Unlike the case of $\gamma = 1$ where we see four final solitons, for $\gamma = 0.5$ we see only two final solitons. It is explained later using the wave functions in the rotated frame. The initial oscillatory dynamics takes place between the two configurations shown in Figs. 13(a) and 13(b). Figure 13(b) is a completely miscible state with peaks of $|\psi_{\pm1}|^2$ that coincide with that of $|\psi_0|^2$. During the oscillatory dynamics, each spin component leaves a small trail of atoms on the opposite sides, i.e., $m = \pm1$ in the right region and $m = 0$ in the left region. Eventually, they cause the formation of a pair of oscillatons. Figures 13(c) and 13(d) show densities at two different instants after the oscillatons are formed. The total density $n(z,t)$ of each oscillaton is identical at both instants, as expected, whereas the density of each component varies in time due to the spin mixing. It is observed that the frequency of internal oscillations of the two oscillatons can be controlled by the extent of overlap Δ. Since $\langle p \rangle = 0$, the denser oscillaton travels slower than the other.

Before the oscillatons are formed, the whole system reaches a miscible state. The density pattern of this miscible state is susceptible to the initial noise in the system, if any is present. The latter can affect the properties of the final oscillatons, such as the mass asymmetry, velocities, and the frequency of the internal oscillations, but general qualitative features of the dynamics remain the same.

For $\phi_1 = 0$, the initial states in the rotated frame are given by the two-soliton solutions in Eq. (19). For $\gamma = 0.5$, in the rotated frame, we have a binary condensate with attractive intra- and intercomponent interactions governed by Eq. (17). Therefore, both $\psi_1'(z)$ and $\psi_{-1}'(z)$ have the tendency to stick

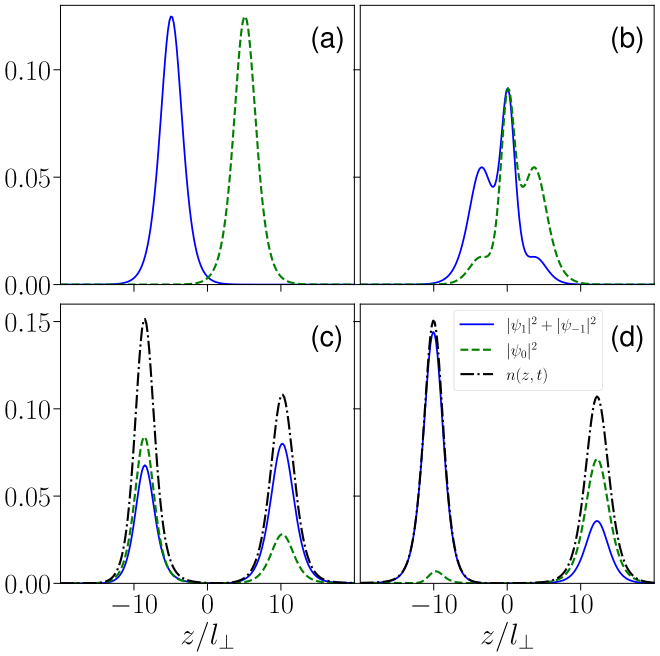

FIG. 13. (a) Snapshot of the initial state of two polar solitons. (b) Snapshot of densities at $\omega_\perp t = 220$. (c) Density profile of the left oscillaton at $\omega_\perp t = 420$. (d) Density profile of the right oscillaton at $\omega_\perp t = 445$. For all plots $\gamma = 0.5$, $\Delta = 10 l_\perp$, $\bar{c}_0/\hbar\omega_\perp l_\perp = -2$, and $\phi_1 = 0$. The solid lines shows $|\psi_1|^2 + |\psi_{-1}|^2$, the dashed lines show $|\psi_0|^2$, and the dash-dotted lines show the total density $n(z)$.

together in the same spatial regions, leading to two final oscillatons or solitons. Note that, unlike in the laboratory frame, an oscillaton is characterized by stationary density profile for each component in the rotated frame, as seen in Figs. 12(d) and 12(e). The wave functions for a stationary oscillation in the rotated frame can be written as $\psi'_{\pm 1}(z) = \eta_\pm \exp[i(\mu_\pm t + \phi_\pm)]$ [24,26], where $\eta_\pm$ satisfy two coupled ordinary differential equations

$$\left(-\frac{\hbar^2}{2m}\frac{d^2}{dz^2} + (\bar{c}_0 + \bar{c}_1)\eta_\pm^2 + (\bar{c}_0 - \bar{c}_1)\eta_\mp^2\right)\eta_\pm = \mu_\pm \eta_\pm. \tag{21}$$

Once we take the two parameters $\mu_\pm$ and $\phi_\pm$ from the original dynamics at an instant, finding the corresponding stationary solutions of the oscillaton is reduced to just solving the ordinary differential equations (21). The latter is done by Euler's method from an initial condition $\eta_\pm \approx 0$ on the left edge and are compared with the original dynamical solutions in Fig. 14. The excellent agreement shown in Fig. 14 confirms that the final solitons formed in the dynamics are oscillatons. In Figs. 14(a) and 14(b) we show the density profiles of $\psi'_{\pm 1}(z)$ for the oscillaton from numerics (dotted lines) and the solution of Eq. (21) (solid and dashed lines) at two different instants. Figure 14(a) is for the left oscillaton and Fig. 14(b) is for the right oscillaton.

Interestingly, for $\phi_1 = 0$, increasing the extent of overlap (decreasing Δ) leads to the emergence of an additional stationary ferromagnetic soliton at $z = 0$ (see Fig. 15). The ferromagnetic soliton exhibits a strong breathing character due to its dynamical formation. Comparing Figs. 15 and 12,

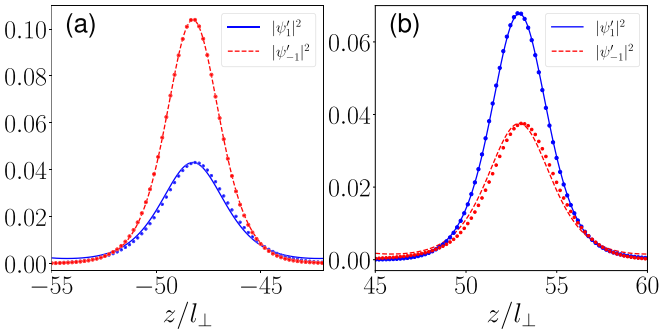

FIG. 14. Density profiles of the oscillaton in the rotated frame at two different instants for the same parameters as in Fig. 13: (a) the left oscillaton and (b) the right oscillaton. The solid $[|\psi'_1(z)|^2]$ and dashed $[|\psi'_{-1}(z)|^2]$ lines show the stationary solution obtained by solving Eq. (21). The dotted line shows the solutions from the dynamics at that particular instant. Both snapshots are taken at $\omega_\perp t = 1000$.

we see that decreasing Δ reduces the frequency of the internal oscillations and increases the velocity of the final oscillatons. Unlike that of $\phi_1 = 0$, the two final oscillatons for $\phi_1 = \pi/2$ rad are symmetric (see Fig. 16). There is no transient oscillatory dynamics at the initial stage of the dynamics because of repulsion emerging from the initial phase difference of $\pi/2$. Also, spin mixing happens independently in the left and right regions due to the initial repulsion. Consequently, we have a pair of identical oscillatons moving away from each other.

4. Case $\gamma \lesssim 1$

We briefly comment on the dynamics when γ slightly deviates from the integrable point $\gamma = 1$. For $\gamma \lesssim 1$ and $\phi_1 = 0$ we see an explicit dependence of Δ on the dynamics. In particular, for $\Delta > \Delta_c$ we see the formation of oscillatons, whereas for $\Delta < \Delta_c$ ferromagnetic solitons emerge. The critical Δ_c becomes larger and larger as γ approaches unity and diverges at $\gamma = 1$. For $\phi_1 = \pi/2$ rad, irrespective of Δ, we observe the formation of oscillatons when γ becomes slightly less than 1. In any case, for nonzero spin-dependent interactions, the overlapping polar solitons convert always to either ferromagnetic solitons or oscillatons.

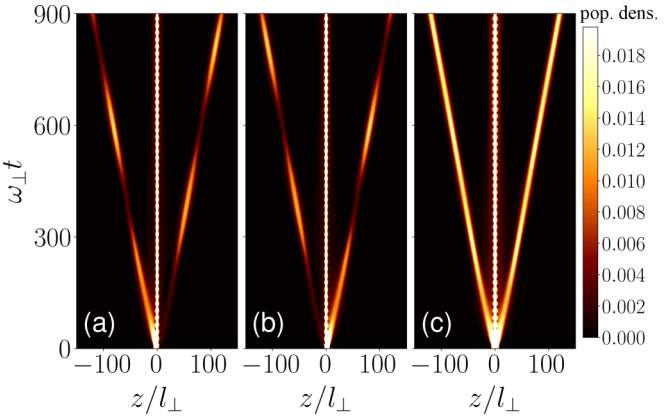

FIG. 15. Population dynamics of two overlapping polar bright solitons for $\gamma = 0.5$, $\Delta = 5 l_\perp$, $\bar{c}_0/\hbar\omega_\perp l_\perp = -2$, and $\phi_1 = 0$ rad: (a) $|\psi_1|^2 + |\psi_{-1}|^2$, (b) $|\psi_0|^2$, and (c) total density $n(z,t)$.

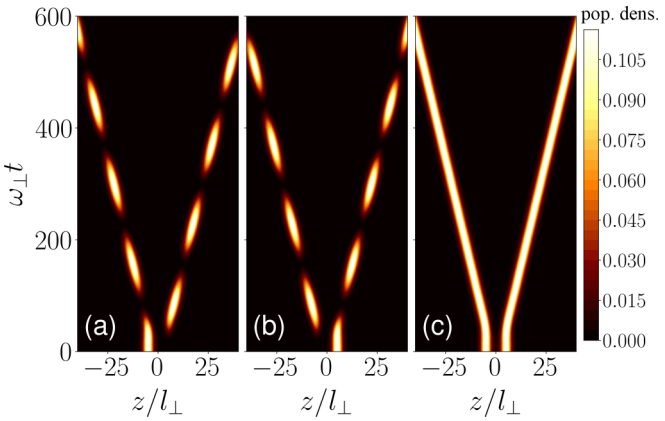

FIG. 16. Population dynamics of two overlapping polar bright solitons for $\gamma = 0.5$, $\Delta = 10 l_\perp$, $\bar{c}_0/\hbar\omega_\perp l_\perp = -2$, and $\phi_1 = \pi/2$ rad: (a) $|\psi_1|^2 + |\psi_{-1}|^2$, (b) $|\psi_0|^2$, and (c) total density $n(z,t)$.

IV. EXPERIMENTAL PROCEDURE

Here we discuss the experimental possibilities of our studies using a rubidium BEC setup in the $F = 1$ state. The necessary steps are shown in Fig. 17. Two state-dependent Q1D harmonic potentials are required [46] in which one confines only $m = \pm 1$ [left one in Fig. 17(a)] atoms and the second traps only $m = 0$ atoms [right one in Fig. 17(a)] and are well separated initially such that the two condensates are physically not connected [see Fig. 17(a)]. A similar trap setup of the spin-1 condensate has been proposed to realize a domain wall between the spin components [47] but not in the bright-soliton regime. In general, the condensates are initially prepared with $c_0 > 0$. One can drive the system to the soliton regime ($c_0 < 0$) using either Feshbach resonance or confinement-induced resonance [48]. In the latter case, the coupling constant becomes

$$g_{\mathcal{F}} = \frac{4\hbar^2 a_{\mathcal{F}} N}{m l_\perp^2}\left(1 - C\frac{a_{\mathcal{F}}}{l_\perp}\right)^{-1}, \tag{22}$$

where $C \approx 1.46$ [49]. The same can be used to tune γ to a desired value. Then, providing a hold time will equilibrate the condensates into two separate stationary polar bright solitons [Fig. 17(b)]. The next step is to bring the two traps closer to an appropriate separation Δ such that they overlap [Fig. 17(c)]. The final step is to imprint the phase difference using additional fields [12,50,51] and remove the traps along the condensate axis to study the dynamics [Fig. 17(d)]. Alternatively, one can implement the method discussed in [42], in which a single bright soliton is split into two solitons with a controlled relative phase and then selectively removing the atoms from other states in each well.

Effect of noise. The nature of noise present in the initial state also depends on the method by which it is prepared. Here we comment on the noise based on the experimental realization discussed above (Sec. IV). Since in the left trap only $m = \pm 1$ atoms are confined, we consider local, tiny random-phase fluctuations (less than $10^{-3}\pi$) on the $m = \pm 1$ components. Similarly, in the right trap, we consider the phase fluctuations only in the $m = 0$ state. We see that such phase fluctuations do not affect the dynamics except in the case of $\gamma = 0.5$ and $\phi_1 = 0$ or π rad and that only quantitatively the qualitative features remain the same.

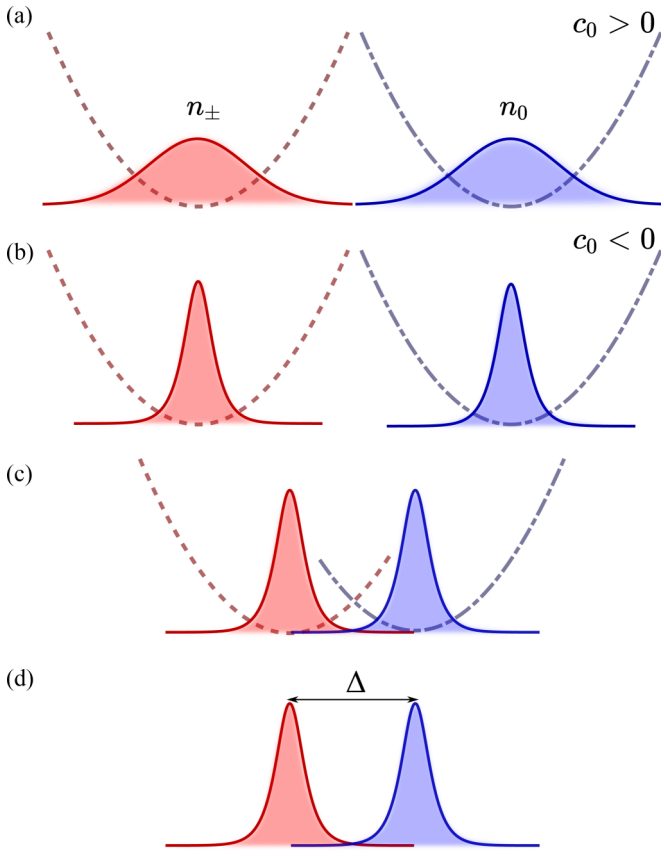

FIG. 17. Experimental procedure for studying the dynamics of overlapping polar bright solitons in a spin-1 condensate. (a) Primary setup, which requires two state-dependent traps in which the left one confines only $m = \pm 1$ atoms and the right one confines only $m = 0$ atoms. (b) In the second step, interaction strength c_0 is varied to $c_0 < 0$ to create the bright solitons. (c) In the third step the traps are closer and thus have an overlap between the solitons. (d) Finally, after imprinting the phase difference, the harmonic trap is released.

V. SUMMARY AND OUTLOOK

We have analyzed the dynamics of two overlapping polar bright solitons in spin-1 condensates, which depends critically on the relative phase, the extent of overlap, and the ratio between spin-independent and spin-dependent interactions. The same dynamics of scalar solitons revealed interesting scenarios, particularly the possibility of observing atomic switching. Atomic switching can find applications in implementing atom-based networks, identical to optical networks. Overlapping polar solitons resulted in nontrivial dynamics in spatial and spin degrees of freedom. For vanishing spin-dependent interactions, we observed Josephson-like oscillations in the densities of each magnetic component. This was explained using an effective double-well potential created by the

density of other components. We observed the formation of four ferromagnetic solitons for identical spin-dependent and spin-independent interactions. When the spin-dependent interaction strength is half the spin-independent one, the dynamics lead to the formation of two oscillatons or a combination of oscillatons and a ferromagnetic soliton. Strikingly, the properties of the final bright solitons can be easily tuned by the initial state and the interaction parameters. Our studies offer a possibility for engineering matter waves. Extending the above analysis to a pair of overlapping ferromagnetic and ferromagnetic-polar solitons, we anticipate exciting dynamics completely different from than those reported here. We also expect complex dynamics to emerge from overlapping more than two solitons.

ACKNOWLEDGMENTS

R.N. acknowledges support from DST-SERB for the Swarnajayanti fellowship File No. SB/SJF/2020-21/19 and National Mission on Interdisciplinary Cyber-Physical Systems of the Department of Science and Technology, Government of India through the I-HUB Quantum Technology Foundation. We acknowledge National Supercomputing Mission for providing computing resources of PARAM Brahma at IISER Pune, which is implemented by C-DAC and supported by the Ministry of Electronics and Information Technology and Department of Science and Technology (DST), Government of India. G.H. acknowledges funding from DST India through INSPIRE-SHE programme.

[1] Y. Kawaguchi and M. Ueda, Phys. Rep. **520**, 253 (2012).
[2] M.-S. Chang, Q. Qin, W. Zhang, L. You, and M. S. Chapman, Nat. Phys. **1**, 111 (2005).
[3] J. Kronjäger, C. Becker, P. Navez, K. Bongs, and K. Sengstock, Phys. Rev. Lett. **97**, 110404 (2006).
[4] A. T. Black, E. Gomez, L. D. Turner, S. Jung, and P. D. Lett, Phys. Rev. Lett. **99**, 070403 (2007).
[5] Y. Liu, S. Jung, S. E. Maxwell, L. D. Turner, E. Tiesinga, and P. D. Lett, Phys. Rev. Lett. **102**, 125301 (2009).
[6] C. Klempt, O. Topic, G. Gebreyesus, M. Scherer, T. Henninger, P. Hyllus, W. Ertmer, L. Santos, and J. J. Arlt, Phys. Rev. Lett. **103**, 195302 (2009).
[7] Y. Eto, H. Shibayama, H. Saito, and T. Hirano, Phys. Rev. A **97**, 021602(R) (2018).
[8] Z. Chen, T. Tang, J. Austin, Z. Shaw, L. Zhao, and Y. Liu, Phys. Rev. Lett. **123**, 113002 (2019).
[9] B. Evrard, A. Qu, J. Dalibard, and F. Gerbier, Phys. Rev. A **103**, L031302 (2021).
[10] H. Pu, C. K. Law, S. Raghavan, J. H. Eberly, and N. P. Bigelow, Phys. Rev. A **60**, 1463 (1999).
[11] T. M. Bersano, V. Gokhroo, M. A. Khamehchi, J. D'Ambroise, D. J. Frantzeskakis, P. Engels, and P. G. Kevrekidis, Phys. Rev. Lett. **120**, 063202 (2018).
[12] X. Chai, D. Lao, K. Fujimoto, R. Hamazaki, M. Ueda, and C. Raman, Phys. Rev. Lett. **125**, 030402 (2020).
[13] A. Farolfi, D. Trypogeorgos, C. Mordini, G. Lamporesi, and G. Ferrari, Phys. Rev. Lett. **125**, 030401 (2020).
[14] S. Lannig, C.-M. Schmied, M. Prüfer, P. Kunkel, R. Strohmaier, H. Strobel, T. Gasenzer, P. G. Kevrekidis, and M. K. Oberthaler, Phys. Rev. Lett. **125**, 170401 (2020).
[15] I. K. Liu, S.-C. Gou, and H. Takeuchi, Phys. Rev. Res. **2**, 033506 (2020).
[16] X. Chai, D. Lao, K. Fujimoto, and C. Raman, Phys. Rev. Res. **3**, L012003 (2021).
[17] G. C. Katsimiga, S. I. Mistakidis, P. Schmelcher, and P. G. Kevrekidis, New J. Phys. **23**, 013015 (2021).
[18] L.-Z. Meng, Y.-H. Qin, and L.-C. Zhao, Commun. Nonlinear Sci. Numer. Simulat. **109**, 106286 (2022).
[19] J. Ieda, T. Miyakawa, and M. Wadati, Phys. Rev. Lett. **93**, 194102 (2004).
[20] J. Ieda, T. Miyakawa, and M. Wadati, J. Phys. Soc. Jpn. **73**, 2996 (2004).
[21] L. Li, Z. Li, B. A. Malomed, D. Mihalache, and W. M. Liu, Phys. Rev. A **72**, 033611 (2005).
[22] E. V. Doktorov, J. Wang, and J. Yang, Phys. Rev. A **77**, 043617 (2008).
[23] V. S. Gerdjikov, N. A. Kostov, and T. I. Valchev, Physica D **238**, 1306 (2009).
[24] P. Szańkowski, M. Trippenbach, E. Infeld, and G. Rowlands, Phys. Rev. A **83**, 013626 (2011).
[25] M. Wang, B. Tian, W.-R. Shan, X. Lü, and Y.-S. Xue, Nonlinear Dyn. **69**, 1137 (2012).
[26] P. Szankowski, M. Trippenbach, E. Infeld, and G. Rowlands, Phys. Rev. Lett. **105**, 125302 (2010).
[27] W. Zhang, O. E. Müstecaplıoğlu, and L. You, Phys. Rev. A **75**, 043601 (2007).
[28] B. A. Malomed, Phys. Rev. A **44**, 6954 (1991).
[29] V. Saxena, I. Kourakis, G. Sanchez-Arriaga, and E. Siminos, Phys. Lett. A **377**, 473 (2013).
[30] V. V. Afanasjev and V. A. Vysloukh, J. Opt. Soc. Am. B **11**, 2385 (1994).
[31] V. V. Afanasjev and N. Akhmediev, Phys. Rev. E **53**, 6471 (1996).
[32] M. Shalaby and A. Barthelemy, Opt. Lett. **16**, 1472 (1991).
[33] M. Shalaby, F. Reynaud, and A. Barthelemy, Opt. Lett. **17**, 778 (1992).
[34] J. S. Aitchison, A. M. Weiner, Y. Silberberg, D. E. Leaird, M. K. Oliver, J. L. Jackel, and P. W. E. Smith, Opt. Lett. **16**, 15 (1991).
[35] I. G. Stegeman and M. Segev, Science **286**, 1518 (1999).
[36] U. Al Khawaja, Phys. Rev. E **81**, 056603 (2010).
[37] U. Al Khawaja, H. T. C. Stoof, R. G. Hulet, K. E. Strecker, and G. B. Partridge, Phys. Rev. Lett. **89**, 200404 (2002).
[38] J. H. V. Nguyen, P. Dyke, D. Luo, B. A. Malomed, and R. G. Hulet, Nat. Phys. **10**, 918 (2014).
[39] T. P. Billam and C. Weiss, Nat. Phys. **10**, 902 (2014).
[40] L. Khaykovich and B. A. Malomed, Phys. Rev. A **74**, 023607 (2006).
[41] N. G. Parker, A. M. Martin, S. L. Cornish, and C. S. Adams, J. Phys. B **41**, 045303 (2008).
[42] T. P. Billam, S. L. Cornish, and S. A. Gardiner, Phys. Rev. A **83**, 041602(R) (2011).
[43] L.-C. Zhao, L. Ling, Z.-Y. Yang, and W.-L. Yang, Nonlinear Dyn. **88**, 2957 (2017).

[44] L. M. Symes, R. I. McLachlan, and P. B. Blakie, Phys. Rev. E **93**, 053309 (2016).
[45] K. L. Lee, N. B. Jørgensen, I. K. Liu, L. Wacker, J. J. Arlt, and N. P. Proukakis, Phys. Rev. A **94**, 013602 (2016).
[46] P. Böhi, M. F. Riedel, J. Hoffrogge, J. Reichel, T. W. Hänsch, and P. Treutlein, Nat. Phys. **5**, 592 (2009).
[47] H. E. Nistazakis, D. J. Frantzeskakis, P. G. Kevrekidis, B. A. Malomed, R. Carretero-González, and A. R. Bishop, Phys. Rev. A **76**, 063603 (2007).
[48] E. Haller, M. J. Mark, R. Hart, J. G. Danzl, L. Reichsöllner, V. Melezhik, P. Schmelcher, and H.-C. Nägerl, Phys. Rev. Lett. **104**, 153203 (2010).
[49] M. Olshanii, Phys. Rev. Lett. **81**, 938 (1998).
[50] S. Burger, K. Bongs, S. Dettmer, W. Ertmer, K. Sengstock, A. Sanpera, G. V. Shlyapnikov, and M. Lewenstein, Phys. Rev. Lett. **83**, 5198 (1999).
[51] J. Denschlag, J. E. Simsarian, D. L. Feder, C. W. Clark, L. A. Collins, J. Cubizolles, L. Deng, E. W. Hagley, K. Helmerson, W. P. Reinhardt, S. L. Rolston, B. I. Schneider, and W. D. Phillips, Science **287**, 97 (2000).